Research Article

Astronomical and atmospheric impacts on deep-sea hydrothermal vent invertebrates

Yann Lelièvre[1,2*], Pierre Legendre[2], Marjolaine Matabos[1], Steve Mihály[3], Claudia P. Arango[4], Raymond W. Lee[5], Pierre-Marie Sarradin[1], Jozée Sarrazin[1]

[1]*Institut Carnot Ifremer EDROME, Centre de Bretagne, REM/EEP, Laboratoire Environnement Profond, F-29280 Plouzané, France.*

[2]*Département de sciences biologiques, Université de Montréal, C.P. 6128, Succursale Centre-ville, Montréal, Québec, H3C 3J7, Canada.*

[3]*Ocean Networks Canada, University of Victoria, PO Box 1700 STN CSC, Victoria, BC V8W 2Y2, Canada.*

[4]*Biodiversity Program, Queensland Museum, PO BOX 3300 South Brisbane QLD 4101, Australia.*

[5]*School of Biological Sciences, Washington State University, Pullman, WA 99164, USA.*

Corresponding author: Lelièvre Yann

Addresses:

(1) Département de sciences biologiques, Université de Montréal, C.P. 6128, Succursale Centre-ville, Montréal, Québec, H3C 3J7, Canada;

(2) Institut Carnot Ifremer EDROME, Centre de Bretagne, REM/EEP, Laboratoire Environnement Profond, F-29280 Plouzané, France.

Telephone number in Canada: (514) 343-7591

Email Address: yann.lelievre@ifremer.fr

Abstract

Ocean tides are considered to be one of the main factors driving the dynamics and spatial structure of marine coastal species but their impacts on deep-sea and hydrothermal vent communities is still limited. Multidisciplinary deep-sea observatories are thus essential to study behavioural rhythms and interactions between hydrothermal community dynamics and environmental fluctuations. Here, we investigated whether species associated with the vent *Ridgeia piscesae* tubeworm assemblage respond to local ocean dynamics. Following variations in vent macrofaunal abundance at different temporal scales, we demonstrated for the first time the impact of tides and surface storms on distribution patterns of mobile and non-symbiotic hydrothermal species (Ammotheidae pycnogonids and Polynoidae polychaetes) at >2 km depth. Ocean dynamics affect the balance between hydrothermal fluid inputs and surrounding seawater, modifying the environmental conditions in vent habitats. We suggest that hydrothermal species react to these habitat modifications by adjusting their behaviour to reach optimal living conditions.

Keywords: Deep-sea observatory, hydrothermal vents, macrofaunal abundance, surface storms, tides, time-series analyses, behavior rhythms.

1. INTRODUCTION

Benthic communities associated with hydrothermal vents have been extensively studied since their discovery in 1977 on the Galápagos ridge [1]. Vent communities, based on local chemosynthetic microbial production, are characterized by low diversity, large biomass and high level of endemic species [2]. Dependent on fluid emissions, hydrothermal species are distributed along an environmental gradient created by the mixing of hot hydrothermal fluids (up to 400 °C) with cold surrounding seawater (<2 °C). Within a single vent site, the high spatial and temporal variability of vent emissions creates a mosaic of habitats characterized by contrasted physical and chemical conditions [3]. The spatial distribution of species results from an interplay between their physiological tolerances to environmental conditions [4–6], resource availability [7,8] and biotic factors [9,10]. Because of their unstable nature, temporal and spatial components of environmental variability play a key role in the functioning of these ecosystems. The diversity and structure of vent communities evolves at different scales in response to the gradient of hydrothermal fluids, which control the successional dynamics of communities [11–13]. Numerous studies also stressed the importance of biological interactions such as predation [9,14], competition [7,9], facilitation [10,15] and inhibition [10,16] on the structure and succession of vent communities.

Hydrothermal ecosystems are variable along a spatial (from cm to hundreds of km) and temporal (from seconds to years) continuum. At broad spatial and temporal scales, the stability of hydrothermal activity and site life span are linked to geodynamic processes such as tectonic or volcanic events [17,18], that can cause important physical, chemical and biological changes [19,20]. At the meter scale, mixing of hydrothermal fluids with seawater creates narrow gradients of environmental conditions [21,22]. Finally, on short temporal scales, high fluctuations of temperature and chemical conditions result from turbulent mixing of hydrothermal fluids and ambient seawater, that are influenced both by variability in hydrothermal fluid flux and local oceanic currents. These deep-sea currents can be forced both astronomically through the periodic variability of surface tides [23–25], and atmospherically by the passage of storms [25,26].

Ocean tides are one of the most important factors controlling intertidal communities [27] but their action on deep-sea communities is less understood. Several studies have shown that physical and chemical conditions in hydrothermal habitats are strongly affected by the tide in the Atlantic [28–30] and Pacific ocean [23,24,31]. Two mechanisms can explain this tidal

98 influence on the hydrothermal environment. (*i*) The modulation of the thickness of the
99 thermal boundary created by the interaction of vent effluent and ambient seawater layer by
100 tidal currents. (*ii*) Direct influence of hydrothermal effluent flux by the effect of pressure of
101 sea-surface and Earth tides on the poro-elasticity of the oceanic crust [23,29]. In addition,
102 winter storms affect bottom currents by generating downward propagating inertial waves and
103 low-frequency currents generated by the pressure fluctuation associated with their passage
104 [32,33].
105
106 Tides may impact faunal distribution by altering the nature and composition of hydrothermal
107 fluids [34–36], but few studies have managed to confirm these hypotheses due to the
108 difficulty of acquiring high-resolution temporal data. To our knowledge, tide influence has
109 only been detected on two symbiotic taxa structuring hydrothermal ecosystems, with: (*i*) an
110 effect on *Bathymodiolus sp*. (Mytilidae, Bivalvia) growth rates [34,37,38] and (*ii*) an impact
111 on *Ridgeia piscesae* (Siboglinidae, Polychaeta) branchial plume movements [36]. Their
112 response to tidal cycles could reflect the variability of seawater mixing with vent fluids,
113 which directly influence the availability of oxygen and energy resources for their symbionts
114 [4].
115
116 Understanding precisely how environmental variability influences vent community dynamics
117 is of particular relevance for hydrothermal biology. To date, only a few studies describing
118 how the activity of vent fauna varies at high frequencies have been published [35,36]. To
119 establish whether the tide plays a role in vent species distributions, the variability of
120 macrofaunal abundance in a *Ridgeia piscesae* siboglinid assemblage from a northeast Pacific
121 hydrothermal edifice was investigated at high temporal resolution. The recent development of
122 deep-sea observatories has allowed for high-resolution *in situ* studies of benthic communities
123 [35,36,39,40]. Video imagery proved to be a good means of studying community dynamics
124 and behaviour [40,41], as well as small-scale changes in activity and faunal distribution
125 [35,36]. This non-invasive method allows for direct observations and provides information on
126 organisms in their natural environment [42]. Since 2009, the Ocean Networks Canada's
127 (ONC's) observatory has provided continuous power and communication to instruments
128 deployed on the seafloor. One of the instrumented arrays is located on the Main Endeavour
129 Field (Endeavour Segment, Juan de Fuca Ridge) and hosts the TEMPO-mini ecological
130 module [43], located on the Grotto edifice (Fig. 1ABC).
131

Based on previous observations [36], we hypothesized that the fauna associated to *Ridgeia piscesae* tubeworms might respond to the tidal signal in response to changes in food availability and environmental conditions. The objectives of the present study are to (*i*) measure environmental conditions in relation to atmospheric and astronomic forcing, (*ii*) determine if species associated with the *R. piscesae* assemblage respond to these forces and (*iii*) assess changes in species activity in relation to variations in environmental conditions.

2. MATERIAL AND METHODS

(a) Study site

The 90-km Endeavour segment located on the northern part of the Juan de Fuca Ridge (JdFR), hosts 5 major hydrothermal vent fields concentrated within a 1-km-wide, 10-km-long rift valley located along the ridge crest [44]. Within the Main Endeavour Field (Fig. 1A), Grotto (47°56.958'N, 129°5.899'W) is a hydrothermal sulphide vent cluster (area ~450 m^2) that forms a cove opened to the north (Fig. 1B), and is one of the most hydrothermally active structures in the Main Endeavour Field [45].

(b) TEMPO-mini ecological observatory module

TEMPO-mini [43] is deployed on the north slope of the Grotto edifice at 2 196 m depth (Fig. 1C) on ONC's NEPTUNE observatory Endeavour node. The module is equipped with an Axis Q1755 camera, four 20W LED lights, an Aanderaa optode coupled with a temperature probe, a 10 m thermistor chain (T-chain) and a CHEMINI chemical analyzer (not installed during our study). The camera and projectors are protected against biofouling by localized microchloration [46]. To study long-term temporal dynamics of vent communities, the camera was programmed to record 20-min video sequences six times a day (at 02 h, 06 h, 10 h, 14 h, 18 h and 22 h UTC) with three zoom changes: "Large", "Medium" and "Fine" views. The camera was focused on a *Ridgeia piscesae* tubeworm assemblage harbouring a dense community of associated fauna. The total studied surface covers approximately 0.315 m^2. In the absence of a 3D model, the observation area was considered to form a two-dimensional surface.

(c) Environmental characterization

Pressure, currents, temperature and oxygen were acquired by instruments installed on or near Grotto (Fig. 1C). Pressure and currents were measured with a highly sensitive bottom

pressure recorder (BPR) and a 600 KHz acoustic Doppler current meter (ADCP) with a useful vertical range of about 30 m, located about 70 m south of Grotto in a flat area without hydrothermal activity. Temperatures were measured by: (*i*) a 25 cm long thermocouple wand (BARS) inserted into a vigorously venting black smoker orifice located about 10 m west of TEMPO-mini, (*ii*) twelve autonomous temperature loggers (F-probes; F1-F12) placed on a tubeworm assemblage, (*iii*) the Aanderaa oxygen sensor deployed 30 to 40 cm below the field of view and (iv) a probe located under a fluid-collection benthic chamber of the remote access fluid sampler (RAS) from a nearby (~1.5 m) diffuse venting area. Oxygen saturation was measured by the Aanderaa optode (see Table S1).

In order to investigate the seasonal component of storms activity in the northeast Pacific Ocean, surface wind stresses (horizontal force of the wind on the sea surface) and wave heights were used as indicators of storm's activity. Data come from a meteorological buoy called "Station 46206 - La Perouse Bank" (48.835 N, 125.998 W; Environnement Canada) located 70 km off the west coast of Vancouver Island. The atmospheric forcing has typical scales of hundreds to thousands of kilometers. Consequently, measurements of winds stress and wave heights by the meteorological buoy are thus a signature of climate variability not only over the local site, but also in the northeast Pacific Ocean.

(d) Observation design

Temporal variations in observed abundances of four taxa (Ammotheidae, Polynoidae, Buccinidae and Zoarcidae) were quantified using large and medium views. To avoid observer bias among consecutive measurements, video sequences were analysed in random order. The first observation strategy had a fixed daily observation time set at 10:00 UTC encompassing a year from 2013-06-20 to 2014-06-20. The second observation strategy was designed to identify seasonal components of macrofaunal and environmental variability. Six observations per day (02:00, 06:00, 10:00, 14:00, 18:00 and 22:00 UTC) were conducted in one summer (June 2014) and two winter (November and December, 2014) months. The selection of these periods was performed in order to minimize the amount of missing data and promote the presence of high-quality video imagery.

(e) Statistical methods

For environmental variables, Welch's averaged modified periodogram method [47,48] was

198 used to identify the dominant periods, and tidal harmonic analysis using open source program
199 t-tide [49] was used to assess the timing (phase of the cycles) and the degree to which the
200 periodicities were determined by tidal forcing. Prior to analysis, the two-dimensional currents
201 were rotated into components along and across the axis of the ridge. The spectra of the
202 currents from fourteen depth ranges from 4 m to 30 m above bottom were examined.
203
204 After substituting missing values using a k-nearest neighbours method in the more sparsely
205 observed macrofaunal abundances time series, Dutilleul's multi-frequential periodogram
206 analysis (MFPA) was used to identify dominant periods [50]. This periodogram computes the
207 variance of periods that do not correspond to an integer number of cycles (fractional
208 frequencies) by the regression on to the sinusoidal representation of the considered frequency.
209 The statistic of Dutilleul's periodogram is defined as the fraction of the total variance of the
210 time series explained by regressing this series on the cosine and sine corresponding to the
211 considered frequency; p-value are produced.
212
213 Using *Piste 3.2.1* (Legendre laboratory, Université de Montréal), path analyses [51] were
214 performed on monthly analyses to investigate how tides affect the variability of macrofaunal
215 abundance. We based the conceptual structure of the path model (Fig. 3) on the hypotheses
216 that near bottom currents influences local environmental conditions (measured variables:
217 temperature and oxygen saturation), that both jointly influence macrofaunal abundance. Thus,
218 the path model had multiple intermediate levels: (*i*) hydrodynamic processes were defined by
219 axial currents, (*ii*) seawater and hydrothermal fluid mixing defined by temperature from the F-
220 probe contributing the most to explaining faunal variability and the single oxygen sensor, and
221 (*iii*) faunal abundance.
222
223 ## 3. RESULTS AND DISCUSSION
224 Ocean tides and surface storms are the main drivers of ocean dynamics [23,26]. These
225 processes create temporal hydrodynamic patterns at different frequencies, which influence the
226 marine ecosystems from coastal zones down to abyssal environment. Using deep-sea cabled
227 observatory approach, we found that the physical and chemical environment of Grotto
228 hydrothermal edifice is strongly influenced by hydrodynamic processes, suggesting a possible
229 influence on vent fauna. Behavioural rhythms studies are essential to understand how species
230 interact with their environment. Widely studied in coastal species, the presence of these
231 rhythms in benthic fauna remains largely unknown [57,58]. A multi-frequential periodogram

analysis computed on observed abundance time series revealed that Ammotheidae pycnogonid and Polynoidae polychaete respond to tides and surface storms. Here, we show for the first time a significantly influence of hydrodynamic processes on distribution patterns of mobile and non-symbiotic hydrothermal species at >2 km depth.

Environmental conditions and ocean dynamics

Most of the environmental measurements were obtained in close proximity to the video-analysed siboglinid assemblage using the cabled instruments of ONC's NEPTUNE observatory (Fig. 1C). Environmental conditions over the study period are summarized in Table S1. Spectral analysis showed that bottom pressure was dominated by peaks in energy centred near frequencies of 1 and 2 cycles per day, the diurnal (12.4 h) and semidiurnal tidal bands (24.8 h) (Fig. 2). The ratio of energy between the near-semidiurnal and near-diurnal bands matched those of barotropic tidal models of the northeast Pacific [52,53] with the near-semidiurnal band being about twice as energetic as the near-diurnal. Similarly, the dominant peak in the current spectra were in the diurnal and semidiurnal bands with the near-semidiurnal band being five times more energetic than the near-diurnal band (Fig. 2). Harmonic analyses of the pressure and current time series revealed that the tidal constituents accounted for 99% and 31% of the variance, respectively. In both instances, the dominant constituent of the near-semidiurnal band was the principal lunar tidal constituent, M_2, at a period of 12.42 h [25], which had three times the amplitude of the second dominant constituent, the principal solar semidiurnal, S_2 at 12 h. In the near-diurnal band, the lunar diurnal constituent K_1 (23.93 h) in both pressure series dominated the solar diurnal constituent P_1 (24.07 h) by a factor of 2.5. We also observed an enhanced energy peak at a 3 to 4 day period and at higher nonlinear harmonics of the tidal frequencies. The shape of the spectrum of currents observed at 4 m above the bottom (mab) through those observed at 30 mab was very similar; however, the total spectral energy increased away from the seafloor by a factor of two from the bottom (4 mab) to the top (30 mab) measurements in the water column. Notable is that the semidiurnal energy was almost entirely concentrated in the along-valley axis component and greatly diminished in the weak cross-axis component (data not shown). The spectra of temperatures and oxygen saturation from a diffuse venting area obtained from the F-probes and Aanderaa optode also revealed significant peaks at the near-semidiurnal and near-diurnal frequencies (Fig. 2). These tidal peaks had less power than those of the pressure and current spectra. Higher nonlinear harmonics of these fundamental tidal peaks were found to varying degrees in several of the spectra. Tidal oscillations were more episodic and less

266 persistent in diffuse fluids than in the high-temperature black smoker fluids, where tidal
267 oscillations were more steady and comparable to the pressure record.
268
269 Looking at the phase relationship among the environmental variables, tidal pressures at Grotto
270 were inversely related to temperature variations of the monitored black smoker. The predicted
271 tide from the pressure and high-temperature time series showed that the end-member (pure
272 hydrothermal) fluid temperature was lower during periods of higher tidal pressure (Fig. S1).
273 Presuming that the change in pressure due to tides forces the change in temperature [54], the
274 phase angle of the dominant predicted tide (M_2 constituent) can be used to estimate the
275 pressure-temperature lag, which at our high-temperature site would be approximately 213°.
276 At the M_2 tidal frequency, this phase lag is about 7.3 h.
277
278 Ambient currents have a complex but direct control on temperature variability in diffuse
279 venting areas and these variations in temperature can be a proxy measurement of the chemical
280 variability of the hydrothermal fluids [55,56]. Since within the rift valley, the dominant
281 periodicity of ambient currents is tidal, we can expect a strong tidal effect on the environment
282 surrounding the faunal community.
283
284 *Impacts of ocean tides on hydrothermal ecosystems*
285 The temporal variability in hydrothermal macrofaunal communities was evaluated in relation
286 to tidal action in the Endeavour rift valley. Dutilleul's periodograms computed on one year of
287 simulated data showed that, with one observation per day, a cosine with 12.4 h tidal period
288 produces a 15-day harmonic. This 15-day period was detected on the observed abundances of
289 Ammotheidae pycnogonids (Table S2), highlighting a tidal signal. For the June, November
290 and December 2014 time series (6 observations per day), periodograms also displayed a
291 significant 12.4 h period corresponding to the semidiurnal tide cycle (Table S2). The observed
292 abundances of Polynoidae polychaetes at the top of the *Ridgeia* bush exhibited a significant
293 tidal cycle (12.4 h) only during the December month (Table S2). Periodograms on Zoarcidae
294 fish abundances did not highlight any significant tide-related periodicity (Table S2).
295 Likewise, periodograms computed on Buccinidae gastropod activity revealed no specific
296 relationship with the tidal signal (Table S2). Successful detection of tidal signals in observed
297 species abundances depends upon the studied time interval, the observation frequency, as well
298 as the abundance and behaviour of the faunal species. When a species is abundant the
299 observer errors causes negligible effects on the observed variability. In contrast, a taxa

represented by a small number of individuals is less likely to display a statistically significant relationship because observer errors increase the variance, creating noise in abundance data. The low number of individuals, combined with the reduced mobility for buccinids, may explain the absence of significant periodicity. Stochastic events (tectonic, volcanic or food inputs), which are common in hydrothermal vents, may also mask an underlying rhythmicity if the response of species to these events is stronger than it is to tides, by generating irregularity in regular biological cycles [59]. Finally, the abundance variations of some taxa might just not be influenced by the tides and associated environmental conditions.

To deepen our understanding of tide-related impacts, we decomposed their relationship with the temporal dynamics of vent macrofaunal communities using path analyses performed on one-month observation periods (Fig. 3). For all the months studied, path analysis results highlighted a strong influence of northern and southern horizontal bottom currents (along-axis currents) on the local physical and chemical conditions of tubeworms habitat. These currents had a strong negative effect on temperature and a strong positive effect on oxygen (Fig. 3). The high influence of northern and southern horizontal bottom currents (valley axis) on local environmental conditions is in concordance with the main orientation of the ridge and topography of the Grotto site. The horseshoe-shaped hydrothermal cluster is opened on the northeast side, directly exposed to north-south current axis (Fig. 1B). The height of the northern towers (10 m) may further protect the assemblage from east/west currents. The tidal modulation of bottom currents is reflected in the fluctuation of current velocities and direction, influencing diffuse flow mixing plumes and therefore, local environmental gradients (Scheirer *et al*. 2006). We show that the tidal forcing causes environmental conditions to alternate between two regimes, which in turn significantly affects the tubeworm assemblage. In particular, the siboglinid habitat fluctuates between warm-low oxygen and cool-high oxygen periods. Temperature is one of the main drivers of vent species distributions and a proxy to trace the turbulent mixing between hot hydrothermal fluids and cold seawater [22,56]. Generally, higher hydrothermal fluid inputs lead to the presence of higher concentrations of hydrogen sulphide and other reduced chemicals (methane, sulphur, metals, etc.) as well as a lower oxygen availability for communities.

Path analyses highlighted a relationship between ocean tides and macrofaunal abundance through the modulation of temperature and oxygen availability by tidal currents (Fig. 3). Highest species abundances were observed during northern current phases (directed to the

334 south) while southern current phases (directed to the north) were characterized by lower
335 faunal abundances. On the environmental slide, the F-probes deployed on the tubeworm
336 assemblage showed that southern current phases were characterised by lower temperatures,
337 hence lower concentrations of hydrogen sulphide and higher oxygen saturation. In these
338 favourable conditions, we hypothesize that species would migrate deeper in the tubeworm
339 bush, protecting themselves against currents and predation, and possibly allocating their
340 energy to other activities such as nutrition and/or reproduction (Fig. 4). Individuals within the
341 tubeworm bush were not visible to the observer, reducing the number of counted individuals.
342 Conversely, the northern current phases were associated with higher temperatures and low
343 oxygen saturation, suggesting higher inputs of hydrothermal fluids in the habitat. We
344 postulate that vent species come to the surface of the tubeworm assemblage in search of more
345 favourable habitat conditions such as higher oxygen saturation (Fig. 4).
346
347 Aggregation and enhanced activity of pycnogonids occurred during higher temperature and
348 lower oxygen saturation periods. In the reverse conditions, pycnogonids were fewer and less
349 active, rendering observations more difficult. This behaviour could be associated to the
350 respiration. In the absence of a respiratory system and pigments that can transport oxygen
351 [60,61], pycnogonids breathe through their exoskeleton by diffusion [62]. Since their cardiac
352 system is too weak to circulate the hemolymph [63], leg joint and peristaltic movements exert
353 pressure on the hemolymph, allowing the oxygen transport [64,65]. Oxygen consumption
354 varies with their activity levels but also with the number of individuals present [66]. Indeed,
355 oxygen consumption is influenced by individuals touching one another and respiration
356 appears to be greater when pycnogonids gather than when they are isolated [66].
357
358 The two endemic polynoid polychaete taxa of the Endeavour vent field (*Branchinotogluma*
359 *sp*. and *Lepidonotopodium piscesae*) showed no distinctive pattern in abundance in relation to
360 tides. Hydrothermal polynoids tolerate a wide range of thermal conditions and the absence of
361 significant influence of temperature on their abundance is in agreement with previous findings
362 that these two species are found within their thermal optimal range [41,67]. In contrast with
363 littoral species, the presence of gills and hemoglobins with high affinity for oxygen in vent
364 polynoids promote oxygen uptake in such hypoxic environments. However, in December
365 2014, polynoid abundance pattern followed a tidal signal in relation with currents. These
366 currents might modulate the availability of food or/and other unmeasured environmental
367 variables but the occurrence of this signal only in December remains to be investigated.

Influence of surface storms on deep-sea fauna

Atmospheric forcing exerts a strong influence on surface ocean dynamics whose effects propagate down to hydrothermal ecosystems. Wind stress and wave height components were plotted for 2014 in order to highlight a seasonal component in storm activity of the northeast Pacific Ocean (Fig. 5). In the summer, wave height is relatively low which is consistent with the reduced wind stresses. However, winter season show a greater instability and suggests an increase of storms activity in the northeast Pacific (Fig. 5).

Ammotheidae and Polynoidae observed abundances responded to local atmospheric forcing with a 4-day oscillation and 16 h inertial oscillation respectively, possibly related to surface storms (Table S2). Evidence of 4-day storm-related oscillations in currents and hydrothermal effluents has been previously reported along the Juan de Fuca Ridge [26,68] and is present in our pressure and current spectra (Fig 2). At the latitude of our study site, the 16 h period corresponds to that of wind-generated inertial currents. When winds at the sea surface are weak or absent, previously induced water movements trace inertia circles because of the Coriolis effect due to the Earth's rotation. Induction of these initial movements may be caused by the passage of storms. This period was previously observed in the times series of Grotto hydrothermal fluxes, showing an influence of surface storms on the dynamics of hydrothermal plumes [69]. However, the environmental variable spectra (Fig. 2) within the rift valley do not reveal significant energy at the 16 h inertial period and we postulate that the narrowness and small size of the rift valley may not permit the entry of internal inertial waves, which are large and propagate at a very small (< 2 deg) angle to the horizontal plane. Conversely, these inertial waves are enhanced above the ridge (~200 mab) [25] where they can periodically advect the neutrally buoyant vent plume and its resident particles. Thus, we postulate that the 4-day oscillations and inertial period (16 h) could be impressed upon the faunal activity by the periodic variability of local environmental conditions and particles settling from the hydrothermal plumes (Fig. 4).

5. CONCLUSION

The influence of astronomical and atmospheric forcing on the ocean generates temporal hydrodynamic patterns whose signatures are found in hydrothermal ecosystems. This study showed for the first time a response of observed abundances of non-symbiotic vent species to

401 the tidal cycle. Our results also revealed an influence of ocean surface storm periodicities
402 during the winter months. These patterns were controlled by near-bottom current variability,
403 which modulates habitat conditions and indirectly influences faunal dynamics. It is now clear
404 that surface ocean dynamics plays a significant role in the functioning of hydrothermal
405 ecosystems.
406
407 An alternative assumption would be the presence of endogenous timekeeping mechanisms,
408 the so-called biological clock. Encoded by clock genes [70], biological rhythms are
409 phylogenetically constrained without being necessarily linked with the presence of cyclic
410 environmental signals. An emerging literature on these endogenous rhythms in deep-sea
411 species suggests an important role of tides in species activity [36,39,58]. Biological rhythms
412 could constitute an anticipated response of organisms to changing environmental conditions
413 caused by ocean variability. In order to test these assumptions, *in vivo* experiments in
414 pressurised aquariums should be investigated.
415

416 ## REFERENCES

417 1. Lonsdale, P. 1977 Clustering of suspension-feeding macrobenthos near abyssal
418 hydrothermal vents at oceanic spreading centers. *Deep. Res. Part I Oceanogr. Res.*
419 *Pap.* **24**, 857–863.

420 2. Tunnicliffe, V. 1991 The biology of hydrothermal vents: ecology and evolution.
421 *Oceanogr. Mar. Biol. Annu. Rev.* **29**, 319–407.

422 3. Sarradin, P.-M., Caprais, J.-C., Briand, P., Gaill, F., Shillito, B. & Desbruyères, D.
423 1998 Chemical and thermal description of the Genesis hydrothermal vent community
424 environment (13°N, EPR). *Cah. Biol. Mar.* **39**, 159–167.

425 4. Childress, J. J. & Fisher, C. R. 1992 The biology of hydrothermal vent animals:
426 physiology, biochemistry, and autotrophic symbioses. *Oceanogr. Mar. Biol. Annu. Rev.*
427 **30**, 337–441.

428 5. Sarrazin, J., Juniper, S. K., Massoth, G. & Legendre, P. 1999 Physical and chemical
429 factors influencing species distributions on hydrothermal sulfide edifices of the Juan de
430 Fuca Ridge, northeast Pacific. *Mar. Ecol. Prog. Ser.* **190**, 89–112.
431 (doi:10.3354/meps190089)

432 6. Luther, G., Rozan, T., Taillefert, M., Nuzzio, D., Di Meo, C., Shank, T., Lutz, R. &
433 Cary, C. 2001 Chemical speciation drives hydrothermal vent ecology. *Nature* **410**,
434 813–816. (doi:10.1038/35071069)

435 7. Levesque, C., Juniper, S. K. & Marcus, J. 2003 Food resource partitioning and

competition among alvinellid polychaetes of Juan de Fuca Ridge hydrothermal vents. *Mar. Ecol. Prog. Ser.* **246**, 173–182. (doi:10.3354/meps246173)

8. De Busserolles, F., Sarrazin, J., Gauthier, O., Gélinas, Y., Fabri, M.-C., Sarradin, P.-M. & Desbruyères, D. 2009 Are spatial variations in the diets of hydrothermal fauna linked to local environmental conditions? *Deep. Res. Part II Top. Stud. Oceanogr.* **56**, 1649–1664. (doi:10.1016/j.dsr2.2009.05.011)

9. Micheli, F., Peterson, C. H., Mullineaux, L. S., Fisher, C. R., Mills, S. W., Sancho, G., Johnson, G. a. & Lenihan, H. S. 2002 Predation structures communities at deep-sea hydrothermal vents. *Ecol. Monogr.* **72**, 365–382. (doi:10.1890/0012-9615(2002)072[0365:PSCADS]2.0.CO;2)

10. Mullineaux, L. S., Peterson, C. H., Micheli, F. & Mills, S. W. 2003 Successional mechanism varies along a gradient in hydrothermal fluid flux at deep-sea vents. *Ecol. Monogr.* **73**, 523–542. (doi:10.1890/02-0674)

11. Shank, T. M., Fornari, D. J., Von Damm, K. L., Lilley, M. D., Haymon, R. M. & Lutz, R. A. 1998 Temporal and spatial patterns of biological community development at nascent deep-sea hydrothermal vents (9°50'N, East Pacific Rise). *Deep. Res. Part II-Topical Stud. Oceanogr.* **45**, 465–515.

12. Sarrazin, J. & Juniper, S. K. 1999 Biological characteristics of a hydrothermal edifice mosaic community. *Mar. Ecol. Prog. Ser.* **185**, 1–19. (doi:10.3354/meps185001)

13. Sarrazin, J., Robigou, V., Juniper, S. K. & Delaney, J. R. 1997 Biological and geological dynamics over four years on a high-temperature sulfide structure at the Juan de Fuca Ridge hydrothermal observatory. *Mar. Ecol. Prog. Ser.* **153**, 5–24. (doi:10.3354/meps153005)

14. Sancho, G., Fisher, C. R., Mills, S., Micheli, F., Johnson, G. a., Lenihan, H. S., Peterson, C. H. & Mullineaux, L. S. 2005 Selective predation by the zoarcid fish Thermarces cerberus at hydrothermal vents. *Deep. Res. Part I Oceanogr. Res. Pap.* **52**, 837–844. (doi:10.1016/j.dsr.2004.12.002)

15. Mullineaux, L. S., Fisher, C. R., Peterson, C. H. & Schaeffer, S. W. 2000 Tubeworm succession at hydrothermal vents: use of biogenic cues to reduce habitat selection error? *Oecologia* **123**, 275–284. (doi:10.1007/s004420051014)

16. Lenihan, H. S., Mills, S. W., Mullineaux, L. S., Peterson, C. H., Fisher, C. R. & Micheli, F. 2008 Biotic interactions at hydrothermal vents: Recruitment inhibition by the mussel Bathymodiolus thermophilus. *Deep. Res. Part I Oceanogr. Res. Pap.* **55**, 1707–1717. (doi:10.1016/j.dsr.2008.07.007)

17. Fouquet, Y., Auzende, J., Ballu, V., Batiza, R., Bideau, D., Cormier, M., Geistdoerfer, P., Lagabrielle, Y. & Sinton, J. 1994 Variabilité des manifestations hydrothermales actuelles le long d'une dorsale ultra-rapide : exemple de la dorsale Est Pacifique entre 17° et 19° S (campagne NAUDUR). *Comptes Rendus l'Academie des Sci. Ser. II* **319**, 1399–1406.

18. Tunnicliffe, V., Embley, R. W., Holden, J. F., Butterfield, D. a., Massoth, G. J. & Juniper, S. K. 1997 Biological colonization of new hydrothermal vents following an eruption on Juan de Fuca Ridge. *Deep. Res. Part I Oceanogr. Res. Pap.* **44**, 1627–1644. (doi:10.1016/S0967-0637(97)00041-1)

19. Juniper, S. K. & Tunnicliffe, V. 1997 Crustal accretion and the hot vent ecosystem. *Philos. Trans. R. Soc. A Math. Phys. Eng. Sci.* **355**, 459–474. (doi:10.1098/rsta.1997.0017)

20. Macdonald, K. C. 1998 Linkages between faulting, volcanism, hydrothermal activity and segmentation on fast spreading centers. *Geophys. Monogr. Geophys. union* **106**, 27–58.

21. Johnson, K. S., Beehler, C. L., Sakamoto-Arnold, C. M. & Childress, J. J. 1986 In situ measurements of chemical distributions in a deep-sea hydrothermal vent field. *Science.* **231**, 1139–1141.

22. Johnson, K. S., Childress, J. J., Hessler, R. R., Sakamoto-Arnold, C. M. & Beehler, C. L. 1988 Chemical and biological interactions in the Rose Garden hydrothermal vent field, Galapagos spreading center. *Deep Sea Res. Part A. Oceanogr. Res. Pap.* **35**, 1723–1744. (doi:10.1016/0198-0149(88)90046-5)

23. Tivey, M., Bradley, A., Terrence, J. & Kadco, D. 2002 Insights into tide-related variability at seafloor hydrothermal vents from time-series temperature measurements. *Earth Planet. Sci. Lett.* **202**, 693–707. (doi:10.1016/S0012-821X(02)00801-4)

24. Scheirer, D. S., Shank, T. M. & Fornari, D. J. 2006 Temperature variations at diffuse and focused flow hydrothermal vent sites along the northern East Pacific Rise. *Geochemistry, Geophys. Geosystems* **7**, 1–23. (doi:10.1029/2005GC001094)

25. Thomson, R. E., Mihály, S. F., Rabinovich, A. B., McDuff, R. E., Veirs, S. R. & Stahr, F. R. 2003 Constrained circulation at Endeavour ridge facilitates colonization by vent larvae. *Nature* **424**, 545–549. (doi:10.1038/nature01814.)

26. Cannon, G. A. & Thomson, R. E. 1996 Characteristics of 4-day oscillations trapped by the Juan de Fuca Ridge. *Geophys. Res. Lett.* **23**, 1613–1616. (doi:10.1029/96GL01370)

27. Connell, J. H. 1972 Community interactions on marine rocky intertidal shores. *Annu. Rev. Ecol. Syst.* **3**, 169–192.

28. Sohn, R. A. 2007 Stochastic analysis of exit fluid temperature records from the active TAG hydrothermal mound (Mid-Atlantic Ridge, 26°N): 2. Hidden Markov models of flow episodes. *J. Geophys. Res. Solid Earth* **112**, 1–16. (doi:10.1029/2007JB004961)

29. Barreyre, T., Escartin, J., Sohn, R. A., Cannat, M., Ballu, V. & Crawford, W. C. 2014 Temporal variability and tidal modulation of hydrothermal exit-fluid temperatures at the Lucky Strike deep-sea vent field, Mid-Atlantic Ridge. *J. Geophys. Res. Solid Earth* **119**, 2543–2566. (doi:10.1002/2013JB010478.Received)

30. Kinoshita, M., Von Herzen, R. ., Matsubayashi, O. & Fujioka, K. 1998 Tidally-driven

effluent detected by long-term temperature monitoring at the TAG hydrothermal mound, Mid-Atlantic Ridge. *Phys. Earth Planet. Inter.* **108**, 143–154. (doi:10.1016/S0031-9201(98)00092-2)

31. Little, S. A., Stolzenbach, K. D. & Grassle, F. J. 1988 Tidal current effects on temperature in diffuse hydrothermal flow: Guaymas basin. *Geophys. Res. Lett.* **15**, 1491–1494.

32. Thomson, R. E., Roth, S. E. & Dymond, J. 1990 Near-inertial motions over a mid-ocean ridge: Effects of topography and hydrothermal plumes. *J. Geophys. Res.* **95**, 7261–7278. (doi:10.1029/JC095iC05p07261)

33. D'Asaro, E. A. 1995 Upper-ocean inertial currents forced by a strong storm. Part III: Interaction of inertial currents and mesoscale eddies. *J. Phys. Oceanogr.* **25**, 2953–2958. (doi:10.1175/1520-0485(1995)025<2953:UOICFB>2.0.CO;2)

34. Nedoncelle, K., Lartaud, F., de Rafelis, M., Boulila, S. & Le Bris, N. 2013 A new method for high-resolution bivalve growth rate studies in hydrothermal environments. *Mar. Biol.* **160**, 1427–1439. (doi:10.1007/s00227-013-2195-7)

35. Sarrazin, J., Cuvelier, D., Peton, L., Legendre, P. & Sarradin, P.-M. 2014 High-resolution dynamics of a deep-sea hydrothermal mussel assemblage monitored by the EMSO-Açores MoMAR observatory. *Deep. Res. Part I Oceanogr. Res. Pap.* **90**, 62–75. (doi:10.1016/j.dsr.2014.04.004)

36. Cuvelier, D., Legendre, P., Laes, A., Sarradin, P.-M. & Sarrazin, J. 2014 Rhythms and community dynamics of a hydrothermal tubeworm assemblage at main endeavour field - A multidisciplinary deep-sea observatory approach. *PLoS One* **9**, e96924. (doi:10.1371/journal.pone.0096924)

37. Schöne, B. R. & Giere, O. 2005 Growth increments and stable isotope variation in shells of the deep-sea hydrothermal vent bivalve mollusk Bathymodiolus brevior from the North Fiji Basin, Pacific Ocean. *Deep. Res. Part I Oceanogr. Res. Pap.* **52**, 1896–1910. (doi:10.1016/j.dsr.2005.06.003)

38. Nedoncelle, K., Lartaud, F., Contreira-Pereira, L., Yücel, M., Thurnherr, A. M., Mullineaux, L. & Le Bris, N. 2015 Bathymodiolus growth dynamics in relation to environmental fluctuations in vent habitats. *Deep Sea Res. Part I Oceanogr. Res. Pap.* (doi:10.1016/j.dsr.2015.10.003)

39. Matabos, M., Bui, A. O. V., Mihály, S., Aguzzi, J., Juniper, K. & Ajayamohan, R. S. 2014 High-frequency study of epibenthic megafaunal community dynamics in Barkley Canyon : A multi-disciplinary approach using the NEPTUNE Canada network. *J. Mar. Syst.* **130**, 56–68. (doi:10.1016/j.jmarsys.2013.05.002)

40. Matabos, M., Piechaud, N., De Montigny, F., Sarradin, P.-M. & Sarrazin, J. 2015 The VENUS cabled observatory as a method to observe fish behaviour and species assemblages in a hypoxic fjord, Saanich Inlet (British Columbia, Canada). *Can. J. Fish. Aquat. Sci.* **72**, 1–13.

552 41. Robert, K., Onthank, K. L., Juniper, S. K. & Lee, R. W. 2012 Small-scale thermal
553 responses of hydrothermal vent polynoid polychaetes: Preliminary in situ experiments
554 and methodological development. *J. Exp. Mar. Bio. Ecol.* **420-421**, 69–76.
555 (doi:10.1016/j.jembe.2012.03.019)

556 42. Cuvelier, D., de Busserolles, F., Lavaud, R., Floc'h, E., Fabri, M.-C., Sarradin, P. M. &
557 Sarrazin, J. 2012 Biological data extraction from imagery - How far can we go? A case
558 study from the Mid-Atlantic Ridge. *Mar. Environ. Res.* **82**, 15–27.
559 (doi:10.1016/j.marenvres.2012.09.001)

560 43. Auffret, Y. et al. 2009 Tempo-Mini: A Custom-designed instrument for real-time
561 monitpring of hydrothermal vent ecosystems.

562 44. Kelley, D. S. et al. 2012 Endeavour Segment of the Juan de Fuca Ridge: one of the
563 most remarkable places on earth. *Oceanography* **25**, 44–61.

564 45. Xu, G., Jackson, D. R., Bemis, K. G. & Rona, P. A. 2014 Time-series measurement of
565 hydrothermal heat flux at the Grotto mound, Endeavour Segment, Juan de Fuca Ridge.
566 *Earth Planet. Sci. Lett.* **404**, 220–231. (doi:10.1016/j.epsl.2014.07.040)

567 46. Delauney, L., Compare, C. & Lehaitre, M. 2010 Biofouling protection for marine
568 environmental sensors. *Ocean Sci.* **6**, 503–511. (doi:10.5194/os-6-503-2010)

569 47. Welch, P. D. 1967 The use of fast Fourier transform for the estimation of power
570 spectra: a method based on time averaging over short, modified periodograms. *IEEE*
571 *Trans Audio* **AU-15**, 70–73.

572 48. Thomson, R. E. & Emery, W. J. 2014 *Data Analysis Methods in Physical*
573 *Oceanography*. Waltham, MA: Elsevier Science.

574 49. Pawlowicz, R., Beardsley, B. & Lentz, S. 2002 Classical tidal harmonic analysis
575 including werror estimates in MATLAB using T_TIDE. *Comput. Geosci.* **28**, 929–937.
576 (doi:10.1016/S0098-3004(02)00013-4)

577 50. Dutilleul, P. 2001 Multi-Frequential Periodogram Analysis and the detection of
578 periodic components in time series. *Commun. Stat. - Theory Methods* **30**, 1063–1098.
579 (doi:10.1081/STA-100104350)

580 51. Wright, S. 1934 The method of path coefficients. *Ann. Math. Stat.* **5**, 161–215.

581 52. Flather, R. A. 1987 A tidal model of the northeast pacific. *Atmosphere-Ocean* **25**, 22–
582 45. (doi:10.1080/07055900.1987.9649262)

583 53. Foreman, M. G. G., Crawford, W. R., Cherniawsky, J. Y., Henry, R. F. & Tarbotton,
584 M. R. 2000 A high-resolution assimilating tidal model for the northeast Pacific Ocean.
585 *J. Geophys. Res.* **105**, 28629. (doi:10.1029/1999JC000122)

586 54. Jupp, T. E. & Schultz, A. 2004 A poroelastic model for the tidal modulation of seafloor
587 hydrothermal systems. *J. Geophys. Res.* **109**, 1–14. (doi:10.1029/2003JB002583)

588 55. Johnson, K. S., Childress, J. J. & Beehler, C. L. 1988 Short-term temperature
589 variability in the Rose Garden hydrothermal vent field : an unstable deep-sea

environment. *Deep Sea Res. Part A. Oceanogr. Res. Pap.* **35**, 1711–1721.

56. Le Bris, N., Rodier, P., Sarradin, P.-M. & Le Gall, C. 2006 Is temperature a good proxy for sulfide in hydrothermal vent habitats? *Cah. Biol. Mar.* **47**, 465–470.

57. Aguzzi, J., Costa, C., Furushima, Y., Chiesa, J. J., Company, J. B., Menesatti, P., Iwase, R. & Fujiwara, Y. 2010 Behavioral rhythms of hydrocarbon seep fauna in relation to internal tides. *Mar. Ecol. Prog. Ser.* **418**, 47–56.

58. Aguzzi, J., Company, J. B., Costa, C., Menesatti, P., Garcia, J. A., Bahamon, N., Puig, P. & Sarda, F. 2011 Activity rhythms in the deep-sea: a chronobiological approach. *Front. Biosci.* **16**, 131–150.

59. Matabos, M., Aguzzi, J., Robert, K., Costa, C., Menesatti, P., Company, J. B. & Juniper, S. K. 2011 Multi-parametric study of behavioural modulation in demersal decapods at the VENUS cabled observatory in Saanich Inlet, British Columbia, Canada. *J. Exp. Mar. Bio. Ecol.* **401**, 89–96. (doi:10.1016/j.jembe.2011.02.041)

60. Redmond, J. R. & Swanson, C. D. 1968 Preliminary studies of the physiology of the Pycnogonida. *Antarct. J. United States* **3**, 130–131.

61. Markl, J. 1986 Evolution and Function of Structurally diverse Subunits in the Respiratory Protein Hemocyanin from Arthropods. *Biol. Bull.* **171**, 90–115.

62. Douglas, E. L., Hedgpeth, J. W. & Hemmingsen, E. A. 1969 Oxygen consumption of some Antarctic pycnogonids. *Antarct. J. United States* **4**, 109.

63. Tjonneland, A., Kland, S. & Nylund, A. 1987 Evolutionary aspects of the arthropod heart. *Zool. Scr.* **16**, 167–175. (doi:10.1111/j.1463-6409.1987.tb00063.x)

64. Davenport, J., Blackstock, N., Davies, D. A. & Yarrington, M. 1987 Observations on the physiology and integumentary structure of the Antarctic pycnogonid Decolopoda austratis. *J. Zool.* **211**, 451–465.

65. Tjonneland, A., Kryvi, H., Ostnes, J. P. & Okland, S. 1985 The heart ultrastructure in two species of pycnogonids, and its phylogenetic implications. *Zool. Scr.* **14**, 215–219. (doi:10.1111/j.1463-6409.1985.tb00191.x)

66. Dresco-Derouet, L. 1978 Métabolisme respiratoire de Nymphon gracile Leach et d'Endeis spinosa (Montagu) (Pycnogonida). *Cah. Biol. Mar.* **19**, 309–315.

67. Bates, A. E., Lee, R. W., Tunnicliffe, V. & Lamare, M. D. 2010 Deep-sea hydrothermal vent animals seek cool fluids in a highly variable thermal environment. *Nat. Commun.* **1**, 1–14. (doi:10.1038/ncomms1014)

68. Cannon, G. A. & Pashinski, D. J. 1997 Variations in mean currents affecting hydrothermal plumes on the Juan de Fuca Ridge. *J. Geophys. Res.* **102**, 24,965–24,976.

69. Xu, G., Jackson, D. R., Bemis, K. G. & Rona, P. A. 2013 Observations of the volume flux of a seafloor hydrothermal plume using an acoustic imaging sonar. *Geochemistry, Geophys. Geosystems* **14**, 2369–2382.

70. Lowrey, P. L. & Takahashi, J. S. 2004 Mammalian circadian biology: elucidating genome-wide levels of temporal organization. *Annu. Rev. Genomics Hum. Genet.* **5**, 407–441. (doi:10.1146/annurev.genom.5.061903.175925)

Data accessibility

The raw data used in this research have been made publically available on Ocean Networks Canada: http://www.oceannetworks.ca.

Competing interests

We have no competing interests.

Authors' contributions

P.M.S., J.S. and R.L. designed the research project and developed the instrumentation. Y.L., P.L., M.M., S.M. P.M.S and J.S. conceived the ideas and contributed to the interpretation of the results. Y.L. collected and analysed data. S.M. analysed and interpreted environmental data. P.L. provided advice about the methods of statistical analysis. C.A. provided assistance in the interpretation of Ammotheidae pycnogonid behaviour. P.L., M.M. and J.S. supervised the research project. All authors assisted in the writing process and revised the manuscript.

Funding statement

This research was supported by a Natural Sciences and Engineering Research Council of Canada (NSERC) research grant to P.L.

Acknowledgments

The authors thank the engineers and technicians who developed and maintain TEMPO-mini (Ifremer RDT, LEP, ONC). Extended thanks go to the captain and crews of the R/V Thomas G. Thompson, the staff of ONC and ROVs ROPOS and Oceaneering Millenium during the deployment and recovery cruises. We are grateful to all PIs of ONC for accessing their temporal data. This work was supported by the "Laboratoire d'Excellence" LabexMER (ANR-10-LABX-19) and co-funded by a grant from the French government under the

program "Investissements d'avenir". We are also grateful to M. Lelièvre, L. Corbari (MNHN, France) and the Québec Centre for Biodiversity Science.

Figure legends

Fig. 1. (A) Location map of the Main Endeavour Field (Juan de Fuca Ridge, Northeast Pacific) indicating the positions of hydrothermal vents edifices, with (B) a visualization of the topographic structure of Grotto. The yellow dot on Grotto represents the position of TEMPO-mini. The distances and height were estimated from COVIS (Cabled Observatory Vent-Imaging Sonar). (C) Deployed instruments: A = Remote Access Sampler (RAS); B = assemblage filmed by TEMPO-mini camera; C = Benthic And Resistivity Sensors (BARS); D = Aanderaa optode; E = TEMPO-mini ecological module; F = thermistor chain (T-chain) and G = autonomous temperature loggers (F-probes).

Fig. 2. Normalised spectra of measured environmental variables with identified periodicity bands. Degrees of freedom used to generate the spectra ranged from 24 to 98 based on length of time series and resolution.

Fig. 3. Path analysis model of ocean tide effects on macrofaunal abundance for one summer (June 2014) and two winter months (November and December 2014). Arrow colour indicates the direction of the effect (black, positive; red, negative). Path coefficients indicate the direct relationships between the different variables and their significance. Significance codes: no significance (ns), (*) $p \leq 0.05$, (**) $p \leq 0.01$ and (***) $p \leq 0.001$. Indirect effects are estimated by multiplying the coefficients of individual segments along paths. The percentages shown in ellipses indicate the proportions of variance explained by the model (adjusted R^2).

682 **Fig. 4.** Schematic representation of tidal and atmospheric forcing on habitat conditions and
683 vent species dynamics. The influence of ocean tides on the observed Ammotheidae
684 abundances followed a 12.4 h cycle (all study periods). In contrast, the effect on observed
685 Polynoidae abundances was felt only during December 2014. In November 2014, observed
686 abundances were additionally impacted by local surface storms with a 4-day (Ammotheidae)
687 and 16 h (Polynoidae) response, respectively. Current variability affects the balance between
688 hydrothermal fluid inputs and the surrounding seawater, modifying the physical and chemical
689 conditions of vent habitat. Hydrothermal species react to these habitat modifications by
690 adjusting their behaviour that is by moving up and down the tubeworm assemblage.
691
692 **Fig. 5.** Surface wind stresses and wave heights in the Northeast Pacific during 2014. These
693 components were used as indicators of storm activity. Shadowed parts in the graphics
694 correspond to the monthly faunal observations analyzed in this study.

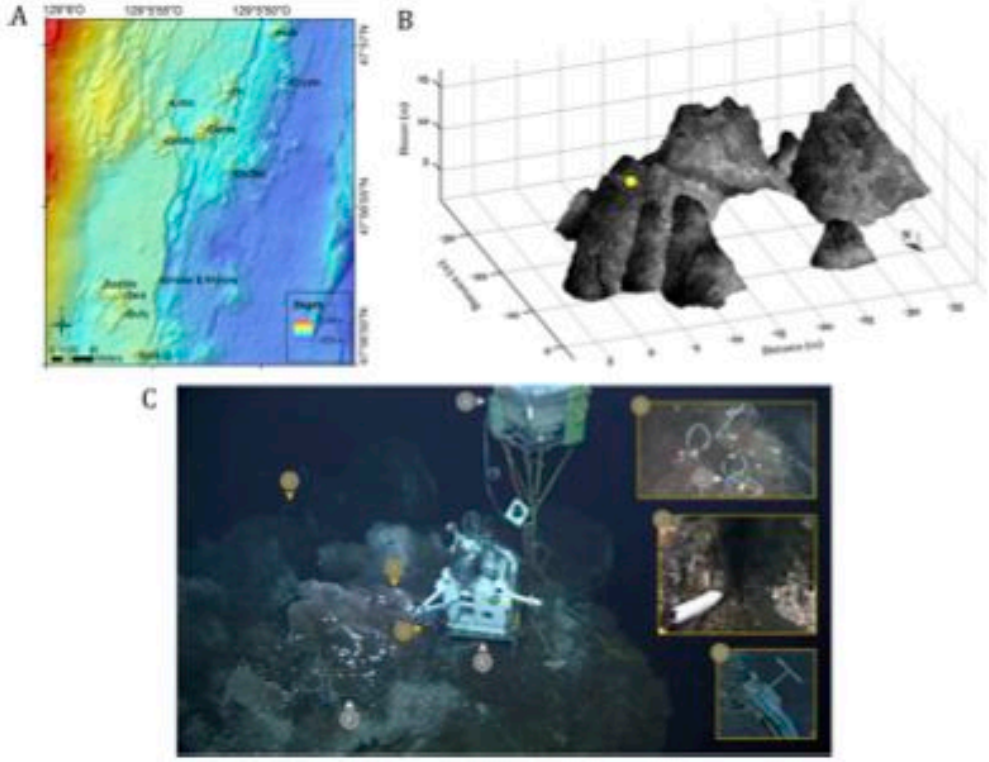
A
B
C

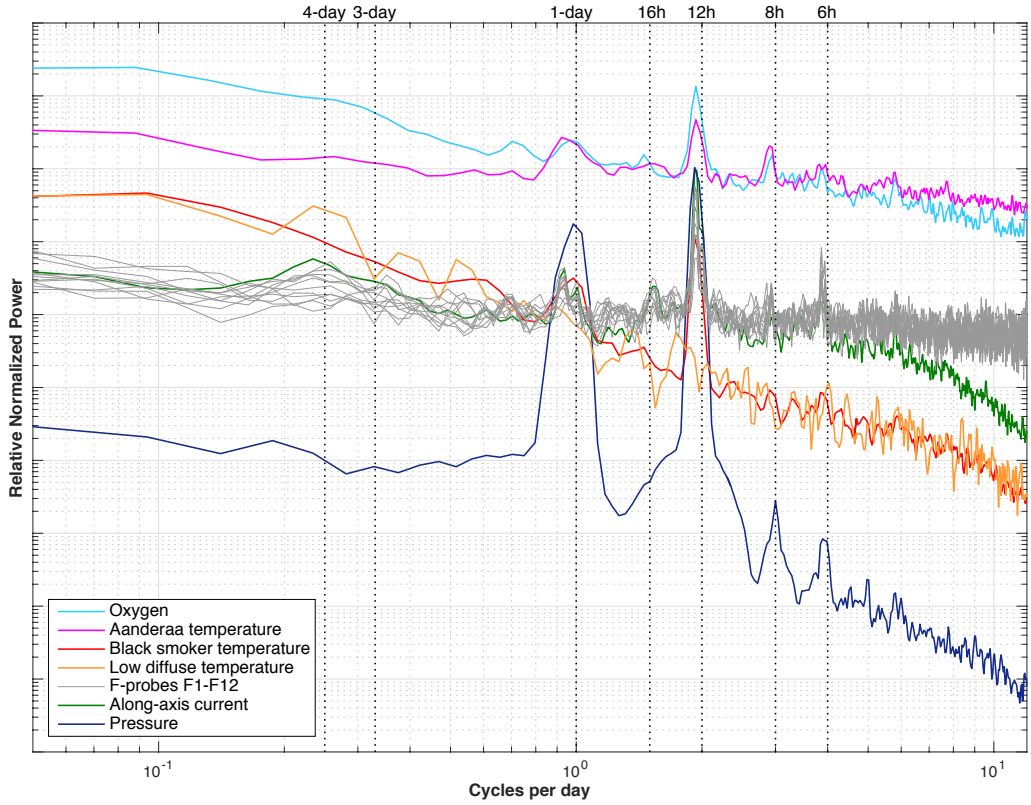
4-day
3-day
1-day
16h
12h
8h
6h
Relative Normalized Power
Cycles per day
10^{-1}
10^{0}
10^{1}
Oxygen
Aanderaa temperature
Black smoker temperature
Low diffuse temperature
F-probes F1-F12
Along-axis current
Pressure

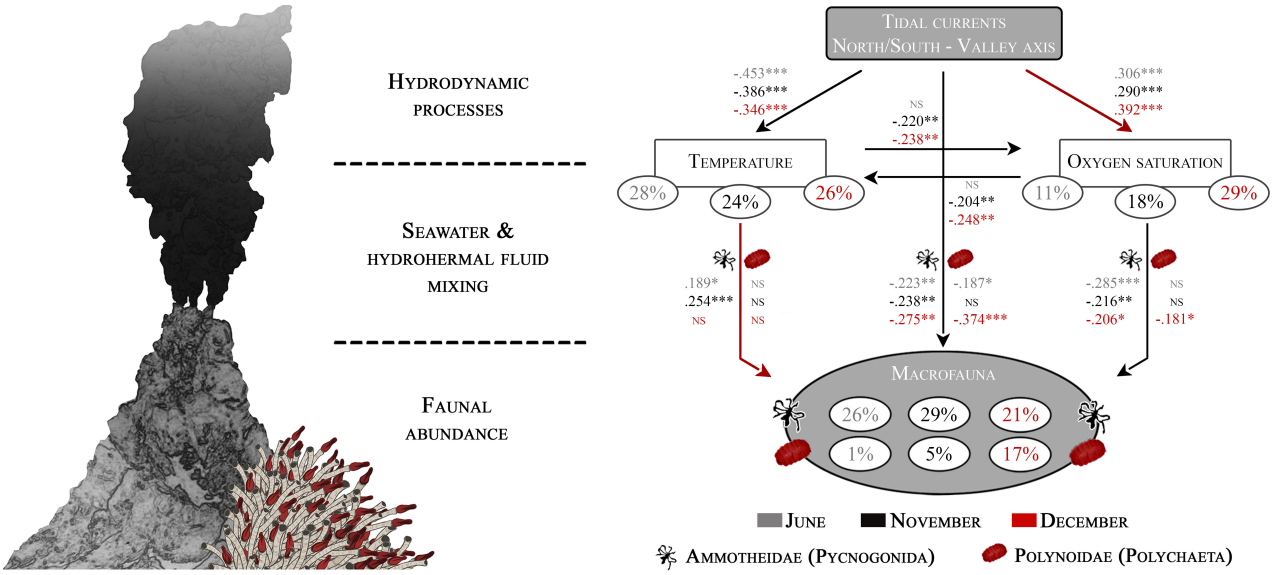
Hydrodynamic processes
Seawater & hydrothermal fluid mixing
Faunal abundance
Tidal currents North/South - Valley axis
-.453***
-.386***
-.346***
NS
-.220**
-.238**
.306***
.290***
.392***
Temperature
Oxygen saturation
28%
24%
26%
11%
18%
29%
NS
-.204**
-.248**
.189*
.254***
NS
NS
NS
NS
-.223**
-.238**
-.275**
-.187*
NS
-.374***
-.285***
-.216**
-.206*
NS
NS
-.181*
Macrofauna
26%
29%
21%
1%
5%
17%
June
November
December
Ammotheidae (Pycnogonida)
Polynoidae (Polychaeta)

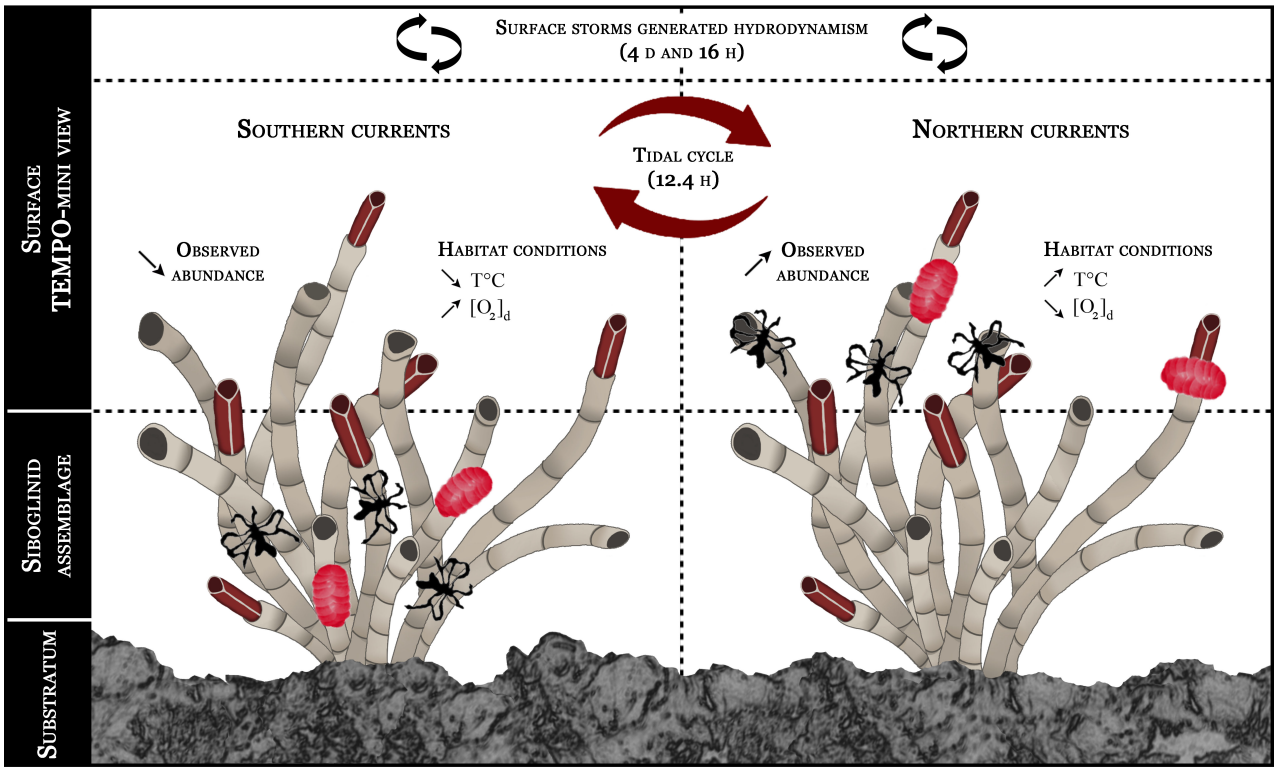
Surface TEMPO-mini view
Siboglinid assemblage
Substratum
Surface storms generated hydrodynamism
(4 d and 16 h)
Southern currents
Tidal cycle
(12.4 h)
Northern currents
Observed abundance
Habitat conditions
↘ T°C
↗ [O2]d
Observed abundance
Habitat conditions
↗ T°C
↘ [O2]d

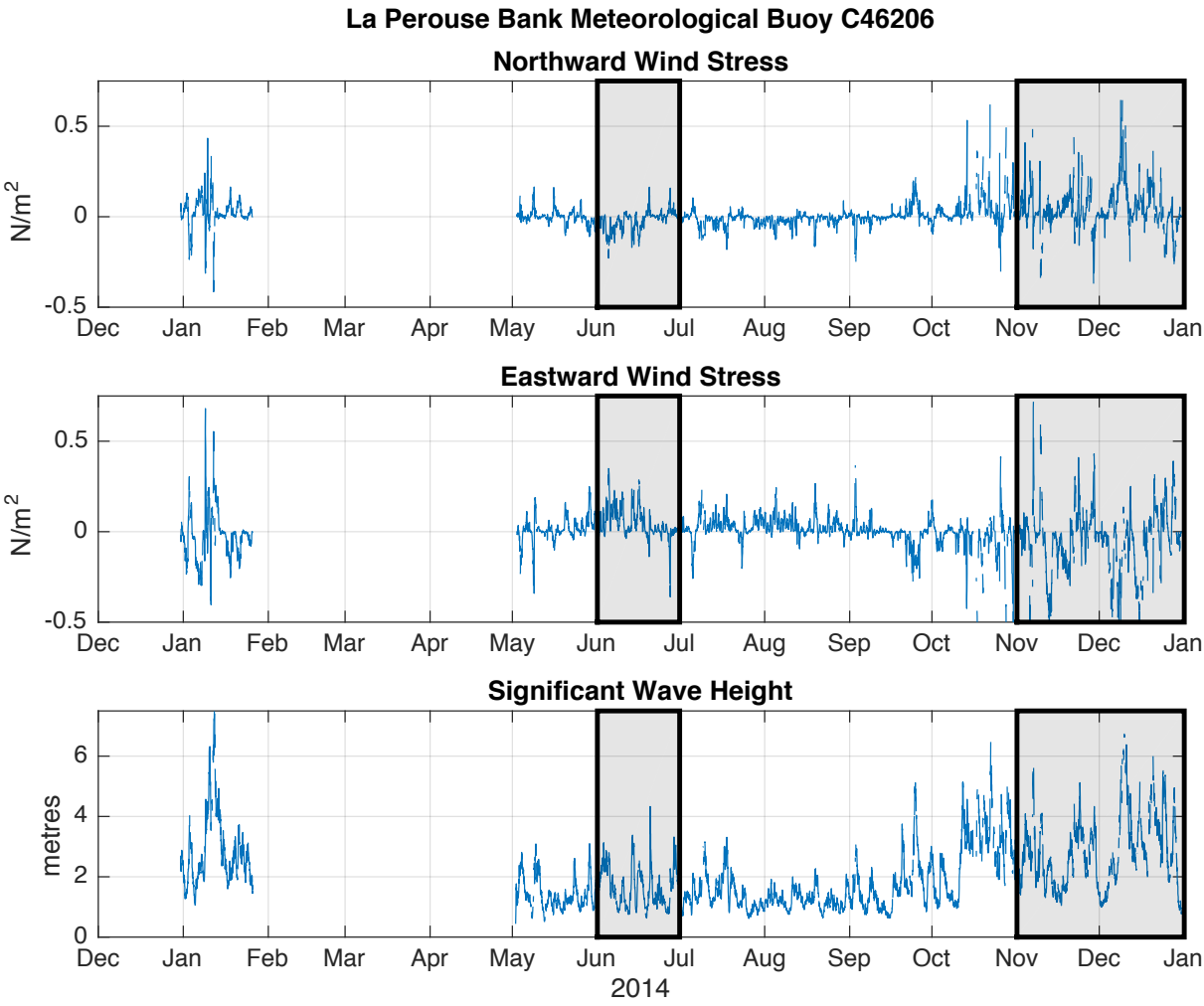
La Perouse Bank Meteorological Buoy C46206
Northward Wind Stress
N/m2
0.5
0
-0.5
Dec
Jan
Feb
Mar
Apr
May
Jun
Jul
Aug
Sep
Oct
Nov
Dec
Jan
Eastward Wind Stress
N/m2
0.5
0
-0.5
Dec
Jan
Feb
Mar
Apr
May
Jun
Jul
Aug
Sep
Oct
Nov
Dec
Jan
Significant Wave Height
metres
6
4
2
0
Dec
Jan
Feb
Mar
Apr
May
Jun
Jul
Aug
Sep
Oct
Nov
Dec
Jan
2014

Supplementary Information for

Astronomical and atmospheric impacts on deep-sea hydrothermal vent invertebrates

Yann Lelièvre[1,2*], Pierre Legendre[2], Marjolaine Matabos[1], Steve Mihály[3], Claudia P. Arango[4], Raymond W. Lee[5], Pierre-Marie Sarradin[1], Jozée Sarrazin[1]

[1]Institut Carnot Ifremer EDROME, Centre de Bretagne, REM/EEP, Laboratoire Environnement Profond, F-29280 Plouzané, France. [2]Département de sciences biologiques, Université de Montréal, C.P. 6128, Succursale Centre-ville, Montréal, Québec, H3C 3J7, Canada. [3]Ocean Networks Canada, University of Victoria, PO Box 1700 STN CSC, Victoria, BC V8W 2Y2, Canada. [4]Biodiversity Program, Queensland Museum, PO BOX 3300 South Brisbane QLD 4101, Australia. [5]School of Biological Sciences, Washington State University, Pullman, WA 99164, USA.

correspondence to: yann.lelievre@ifremer.fr

This PDF file includes:

Supplementary Figure S1

Fig. S1. Phase relationships among the environmental variables.

Supplementary Table S1

Table S1. List of instruments used in this study, summarizing the characteristics, the habitat conditions as well as the periods for each variable of interest, and the principal investigators responsible for the instruments.

Supplementary Table S2

Table S2. Observed abundances and periodic analyses of the hydrothermal vent fauna at the Grotto edifice (2 196 m depth). Data are based on the manual analysis of video images recorded by the TEMPO-mini ecological module.

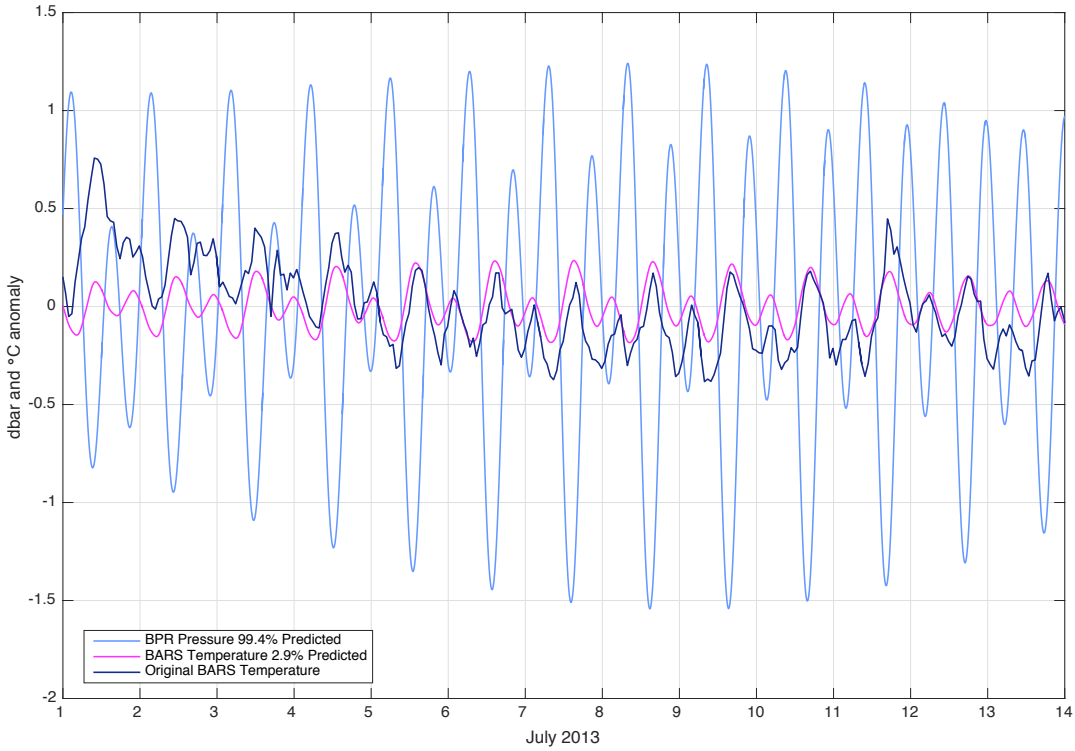
1.5
1
0.5
0
-0.5
-1
-1.5
-2
dbar and °C anomaly
1
2
3
4
5
6
7
8
9
10
11
12
13
14
July 2013
BPR Pressure 99.4% Predicted
BARS Temperature 2.9% Predicted
Original BARS Temperature

Table S1. List of instruments used in this study, summarizing the characteristics, the habitat conditions as well as the periods for each variable of interest, and the principal investigators responsible for the instruments.

Instruments (units)	Sample interval	Acquisition frequency	min-max (mean ± sd)	Main periods	Principal Investigators
BPR (bar) *Bottom Pressure Recorder*	Pressure	1 second	220.03-222.69 (221.32 ± 3.78)	3-4 day 12.4 h and 24.8 h	R.Thomson
ADCP (cm/s) *Acoustic Doppler Current Profiler*	Current	1 second	0.00-20.73 (4.99 ± 2.83)	3-4 day 12.4 h and 24.8 h	S. Mihály
BARS (°C) *Benthic and Resistivity Sensors*	Temperature black smoker	20 seconds	330.43-334.7 (332.58 ± 0.64)	12.4 h 24.8 h	M. Lilley
RAS (°C) *Remote Access Water Sampler*	Temperature diffuse flow	1 second	31.47-74.66 (45.71 ± 5.76)	12.4 h 24.8 h	D. Butterfield
F-probes (°C) F1-F12	Temperature Siboglinidae assemblage	1 hour	1.6-13.6 (3.9 ± 0.6)	12.4 h 24.8 h	R. Lee
Andearaa Optode Temperature (°C)	Temperature Siboglinidae assemblage	30 seconds	1.93-4.96 (2.7 ± 0.32)	12.4 h 24.8 h	P-M. Sarradin
Andearaa Optode Oxygen (% saturation)	Oxygen Siboglinidae assemblage	15 minutes	1.53-22.07 (11.56 ± 3.35)	12.4 h 24.8 h	P-M. Sarradin

Table S2. Observed abundances and periodic analyses of the hydrothermal vent fauna at the Grotto edifice (2 196 m depth). Data are based on the manual analysis of video images recorded by the TEMPO-mini ecological module.

Taxa	Annual analysis		Monthly analyses					
	2013-06-20 to 2014-06-20		June 2014		November 2014		December 2014	
	min-max (mean ± sd)	Main periods	min-max (mean ± sd)	Main periods	min-max (mean ± sd)	Main periods	min-max (mean ± sd)	Main periods
Ammotheidae	2-31 (14.7 ± 5.85)	15 day	14-46 (24.32 ± 5.62)	12.4 h	15-48 (26.75 ± 5.57)	4 day 12.4 h	9-37 (23.65 ± 5.36)	12.4 h
Polynoidae	1-34 (8.57 ± 3.53)	-	4-20 (10.81 ± 3.47)	-	7-24 (14.68 ± 3.6)	16 h	7-25 (14.36 ± 3.86)	12.4 h
Buccnidae	4-22 (12.2 ± 3.13)	-	8-22 (14.99 ± 2.56)	-	12-22 (17.12 ± 2.19)	-	8-22 (15.16 ± 2.73)	-
Zoarcidae	0-6 (1.66 ± 1.22)	-	0-5 (1.42 ± 1.05)	-	0-4 (0.74 ± 0.85)	-	0-4 (0.92 ± 0.96)	-